ACS APPLIED POLYMER MATERIALS

pubs.acs.org/acsapm Article

Toughening Poly(methyl methacrylate) via Reinforcement with Cellulose Nanofibrils

Gnana Saurya Vankayalapati, Ethan Kaplan, Lisa M. Lallo, Nikhil Victor, Craig M. Clemons, John M. Considine, and Kevin T. Turner*

Cite This: *ACS Appl. Polym. Mater.* 2021, 3, 6102–6110 Read Online

ACCESS | Metrics & More | Article Recommendations | Supporting Information

ABSTRACT: The incorporation of fibers into polymers is a well-known route for realizing composite materials with improved strength, stiffness, and toughness. Cellulose nanofibrils (CNFs) are a promising reinforcement because of their high aspect ratio, high specific stiffness and specific strength, and transparency and the fact that they are derived from renewable and sustainable sources. Here, we demonstrate the application of CNFs for the reinforcement of continuous polymer fibers (filaments) to achieve a concurrent enhancement of strength, stiffness, and fracture toughness. Poly(methyl methacrylate) (PMMA)-CNF composite fibers with 0 to 3 wt % CNFs were made by solvent blending and melt-spinning/drawing techniques, resulting in fibers with diameters ranging from 200 to 300 μm. The processing route was developed to overcome challenges presented by the combination of high processing temperatures of PMMA and the low thermal stability of CNFs as well as the formation of a percolated CNF network and low volume fractions. Fourier transform infrared (FTIR) spectroscopy was used to understand the alignment of PMMA and CNFs in the fibers. The strength and Young's modulus of the fibers were characterized by tensile testing, and the fracture toughness was measured via notched fiber tests. The addition of low-weight fractions (<3%) of CNFs increased Young's modulus by 35% and yield strength by 19% compared to neat PMMA fibers. Along with this increase in stiffness and strength, the incorporation of 1 wt % CNF led to a doubling of the fracture toughness. FTIR results and imaging of the fracture surfaces provided insight into toughening mechanisms.

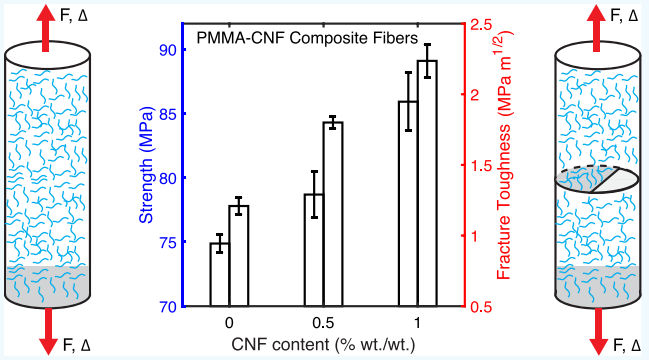

KEYWORDS: *nanocellulose, cellulose nanofibrils, PMMA, composite fibers, mechanical properties, fracture toughness*

INTRODUCTION

Cellulose nanofibrils (CNFs) are derived from cellulose, the world's most abundant natural polymer. CNFs come from sustainable and renewable sources and have high aspect ratios, are transparent, and have excellent mechanical properties[1,2] that make CNFs attractive for use in structural materials. CNFs offer potential as a reinforcing phase to enhance the mechanical properties of polymer materials. For example, Seydibeyoglu and Oksman[3] and Leng and Pan[4] demonstrated improvement in the elastic modulus and tensile strength of polyurethane/CNF composites. Zhang et al.[5] and Venugopal and Gopalakrishnan[6] showed enhancement of tensile strength and tear strength of natural rubber through reinforcing with CNFs extracted from eucalyptus kraft pulp and coconut spathe, respectively.

In addition to improvements in modulus and strength, incorporation of CNFs into polymers can potentially improve the fracture toughness, which is a measure of the material's resistance to crack growth. Fracture toughness is a critical property in the selection of materials for load-bearing materials, and enhancing fracture toughness is, in general, challenging,[7] especially without adversely affecting strength. However, composite materials provide potential to engineer materials with both high toughness and strength. This is achieved through mechanisms such as fiber bridging across the crack and fiber pullout. Nanocomposites, in which the reinforcing phase has at least one dimension smaller than 100 nm, have attracted interest because of the high strength of nanoscale fibers because of low defect density and high surface-to-volume fractions, which allow manipulation of stress transfer between the matrix and the fibers.[8,9]

Poly(methyl methacrylate) (PMMA), also known as acrylic, is a commonly used thermoplastic with moderate toughness and is widely used in many engineered products and systems because of its manufacturability and transparency. Therefore,

Received: July 28, 2021
Accepted: October 11, 2021
Published: November 8, 2021

enhancing the fracture toughness of PMMA is an essential task. The toughness of polymer composites can be improved through nanofiber-reinforcement.[10,11] Sui and Wagner[12] demonstrated an increase in strength, modulus, and tensile toughness of PMMA via the addition of multiwalled carbon nanotubes. However, carbon nanotubes are expensive and affect the transparency of PMMA. CNFs offer a renewable and sustainable alternative while maintaining good optical properties.

CNF reinforcement has the potential to increase toughness while maintaining the optical transparency of the composite material. Such composites have been investigated by several others, and CNFs have been shown to positively influence mechanical performance. However, the results are mixed and inconsistent, and properties such as fracture toughness have not been evaluated. For example, Kiziltas et al.[13] showed that adding small amounts (0.5% or less) of highly fibrillated cellulose had little effect on flexural modulus or strength. However, a large increase in strain to failure was found at 0.5% but not at 0.25% cellulose addition. Also, the coarseness of the cellulose adversely affected the transparency of PMMA. Dong et al.[14] found large increases in failure strain and tensile toughness of PMMA with additions of 1 and 3% CNF but far less and none at 0.5 and 5% CNF, respectively. Modulus and strength were reduced with addition of small amounts of CNFs, but these losses were largely recovered once the CNF content was increased to about 3−5%. Transparency was largely retained with CNF addition. Banerjee et al.[15] showed that surface treatment of CNFs in methyl methacrylate (MMA) resulted in better dispersion in PMMA. An increase of 15% in strength and 39% Young's modulus were reported on addition of 1% surface-modified CNFs. Oliver-Ortega et al.[16] formulated composites of PMMA and nanofibers of kombucha bacterial cellulose and found a 200% improvement in Young's modulus but tensile strength and strain at failure reduced by 13 and 78%, respectively.

Widely varying results from these investigations are likely due to differences in CNF and composite preparation and warrant further exploration. Also, these earlier investigations primarily examined solvent-blended, cast films. Such approaches require removal of large amounts of organic solvents and are more expensive and less environmentally preferable than the more conventional melt-processing methods. Moreover, none of these previous studies on PMMA-CNF composites have characterized fracture toughness, which is measured for specimens containing an initial crack. While fracture toughness is often positively correlated with tensile toughness values (i.e., the area under the stress stain curve) for some materials, fracture toughness is a distinct quantity that describes a material's damage tolerance and is frequently used in mechanical design. Here, we examine the effects of composite preparation and further investigate the mechanical behavior of these composites, especially the fracture toughness. While PMMA and CNF were still compounded via solvent blending to ensure good dispersion, the possibility of melt processing was assessed via melt spinning of fibers and hot drawing. Tensile tests were performed to determine elastic modulus and yield strength, and the mode I fracture toughness of the composite fibers was determined from specimens that were precracked by a microindentation procedure.

EXPERIMENTAL SECTION

Materials. PMMA with a molecular weight of 120,000 and N,N dimethylformamide (DMF) were obtained commercially (Sigma-Aldrich). TEMPO-oxidized CNFs with aspect ratios >100 and approximately 10 nm in diameter were produced at the USDA Forest Products Laboratory. The detailed preparation technique of CNFs using TEMPO (2,2,6,6-tetramethylpiperiding-1-oxly-radical) pretreatment has been described previously.[17,18] To break up remaining agglomerates found by polarized light microscopy, the CNFs were passed an additional three times through a homogenizer (Microfluidics M-110EH-30) equipped with 200 and 87 μm orifices in series.

Fabrication of PMMA-CNF Composite Fibers. The aqueous dispersion of CNFs was solvent-exchanged with DMF by vacuum-assisted rotary evaporation by a method similar to that used by Dong et al.[14] Briefly, DMF was added to the aqueous CNF dispersion to yield a 3:1 DMF/H_2O wt ratio. The dispersion was then sonicated for approximately 2 min until no gel particles were present. Water was then removed using a rotary film evaporator, and the resulting dispersion was again sonicated for approximately 5 min until no gel particles were present. A final CNF concentration of 0.45 wt % in the solvent-exchanged dispersion was gravimetrically determined after oven drying at 60 °C for 1 week. PMMA was then added to the CNF dispersion. The mixture was stirred at 60 °C for 1 h and then cast into heated glass trays to evaporate the solvent. By adding appropriate ratios of solid PMMA and the CNF dispersion, mixtures were prepared to yield PMMA nanocomposite films containing between 0 and 3% CNF by weight. The PMMA/CNF/DMF mixtures were dried at 70 °C for 4 h and then at room temperature overnight. The resulting films were then removed from the glass trays, Wiley-milled using a 10-mesh screen, and then oven-dried at 60 °C for approximately 1 week until a constant glass transition temperature (T_g) was obtained.

Continuous fibers were then melt-spun from the solvent-blended materials using a microcompounder and fiber spinning line (DSM Xplore, The Netherlands). Barrel temperatures for the feed, middle, and die zones were 190, 200, and 210 °C, respectively, for spinning of the as-received PMMA. The limited thermal stability of the CNF necessitated lowering the spinning temperatures 10 °C from those used for the original PMMA. For consistency, the same lower temperature profile was used for spinning the PMMA that had first been dissolved in PMMA (0% CNF blend). The resulting melt temperatures were 210 and 192 °C for the original PMMA and solvent-blended materials, respectively. Nitrogen blanketing was used to minimize degradation of the CNF. The material was fed into the extruder using a volumetric feeder (MCMicro Ultra compact dosing unit, Movacolor, The Netherlands), and a take up speed of 30 m/min was used for the winding unit. After melt spinning, the resulting composite fiber was further drawn in a second step using the DSM Xplore Conditioning (i.e., drawing) Unit. The original PMMA was drawn at 135 °C, and all solvent-blended materials were drawn at 125 °C at a speed of 100 cm/min. The resulting composite fibers had diameters in the range of 200−300 μm. The composition of the CNF in the final composite fibers was 0.5, 1.0, and 3.0% by weight which approximately corresponds to 0.4, 0.8, and 2.4% by volume, respectively (assuming that the density of PMMA is 1200 kg/m^3 and the density of CNFs is 1500 kg/m^3).

Characterization. The glass transition temperature (T_g) was determined according to ASTM D3418-15[19] using a DSC 7 differential scanning calorimeter (PerkinElmer). Samples were first Wiley-milled using a 10 mesh screen, and then approximately 10 mg of the powder was sealed in an aluminum capsule and heated at 20 °C/min in a nitrogen environment from 30 to 200 °C. The samples were then cooled to 30 °C at 20 °C/min and then held for 5 min at 30 °C. The heating/cooling cycles were then repeated twice for a total of three cycles. T_g was determined as the temperature at which half of the change in specific heat capacity had occurred during the heating cycle.

For dichroic ratio measurements, polarized Fourier transform infrared (FTIR) spectroscopy in the transmission mode was

https://doi.org/10.1021/acsapm.1c00933
ACS Appl. Polym. Mater. 2021, 3, 6102−6110

performed on 25 μm-thick longitudinal sections microtomed from the center of the fibers. The measurements were performed using a Nicolet iN10 MX Infrared imaging microscope equipped with a zinc selenide linear polarizer (Thermo Scientific). The dichroic ratio ($R = A_{\parallel}/A_{\perp}$) is defined as the ratio of peak intensities parallel and perpendicular to the polarization direction of the infrared beam and scales proportionally with molecular orientation. Because of peak overlap between the PMMA and CNF in other areas of the spectra, the peak at a wavelength of 749 cm^{-1} (skeletal CH_2 vibration) was chosen to investigate the orientation of PMMA in the fibers following the method of Andersson et al.[20]

The mechanical properties of the fibers were characterized using a uniaxial testing machine in displacement control (Criterion Model 43, MTS) equipped with a 50 N load cell (LSB.501, MTS) and a digital camera (Guppy Pro, Allied Vision) fitted with a manual focus lens (HR F2.8/50 mm, Navitar) for marker tracking. Fibers were mounted onto specially designed acrylic grips for testing as shown in Figure S1. The design for these acrylic grips was inspired from previous work reported in ASTM C1557[21] using cardboard tabs, Adusumalli et al.[22] using paper frame tabs, and Kant and Penumadu[23] using aluminum templates. The design of the acrylic grips was optimized through iteration to ensure that the fibers fail in the gauge region rather than at the adhered ends. A commercial epoxy (JB Weld) was used to attach the fibers to the acrylic grips. An elastomer (polydimethylsiloxane) was then added at both ends of the fiber to reduce the stress concentrations at the epoxy attachment point and thus facilitate failure in the gauge section of the fiber. Tensile tests of different samples were performed at room temperature of 23 °C and a displacement rate of 40 mm/min (a strain rate of 1 min^{-1}). Around 15−20 specimens of each CNF composition were tested. The thicknesses of the specimens were measured using a digital micrometer. Prior to testing, 1 mm × 1 mm paper markers were attached to the fibers with a dry adhesive for displacement tracking. Paper markers were selected over ink markers because of potential complications that could arise from using water- or solvent-based ink markers. The support arms at the sides of the acrylic fixture were removed prior to testing. During testing, the camera recorded the gauge region at 14 frames per second. Strains during the test were determined by tracking the displacement of the markers on the specimen with respect to an initial reference image.

Representative stress−strain curves for the composite fibers are shown in Figure S2. Displacements (and therefore strains) were calculated by tracking markers on the fibers during testing. To consistently determine the mechanical properties of the fibers, the stress σ, and strain ε, data were fit with a hyperbolic tangent curve, given by eq 1[24] and previously used by Baez et al.,[25]

$$\sigma = B_1 \tanh(B_2*(\varepsilon - B_3)) + B_4*(\varepsilon - B_3) \quad (1)$$

where B_1, B_2, B_3, and B_4 are fitting parameters. The shape of the function and stress magnitude at low strains are captured by B_2 and B_1, respectively. In particular, B_2 is influenced by the strain at yield. The strain offset is determined by B_3. At high strains, the shape of the function is captured by B_4. The derivative of this function evaluated zero strain, which is defined as the initial modulus, E

$$E = B_1*B_2 + B_4 \quad (2)$$

For determining mode I fracture toughness of the fibers, precracks were fabricated using a custom-built microindenter. The aim was to obtain a cut through the cross section of the fiber as shown in Figure S3. A scalpel blade (8 mm × 0.5 mm ceramic scalpel blade, Fine Science Tools) was used to produce sharp cracks with a crack width less than 10 μm. The precrack length was controlled by monitoring the force−displacement curve during blade indentation. The blade was indented at 0.01 mm/s—this slow rate ensured sufficient control for a consistent precrack size. The blade came in contact with the fiber and then was indented until it reached the specified target load, which corresponded to a specific precrack length.

These notched (precracked) fiber specimens were mounted onto acrylic grips using a commercial epoxy (JB Weld) and tested in the tensile testing machine. Peak loads at fracture were recorded and analyzed with a fracture mechanics model (described below) to obtain the fracture toughness of the fibers. Scanning electron microscopy (SEM) was used to image the fracture surfaces of the fibers postfailure, and these images along with other testing conditions were used to determine the type of fracture in these fibers, thereby aiding in the selection of an appropriate fracture model to determine the fracture toughness.

RESULTS AND DISCUSSION

Fiber Preparation. PMMA and CNFs were first compounded by solvent blending in DMF. One of the challenges of solvent blending is complete removal of the solvent because the residual solvent can lower the glass transition temperature T_g and plasticize the polymer, affecting mechanical properties. For example, Patra et al.[26,27] demonstrated how residues of different organic solvents affect the thermal and mechanical properties of cast PMMA films. To remove as much of the DMF as possible, we dried our solvent-blended compounds under vacuum at 60 °C until a constant T_g was achieved, which took approximately 1 week.

Differential Scanning Calorimetry (DSC) Results. The T_g values of the specimens measured over three successive temperature cycles to 200 °C by DSC are summarized in Table 1. The first heating cycle T_g values for the solvent-blended composites as well as the increasing trend with CNF addition are similar to those found by Dong et al.[14] Comparing the T_g values of as-received ("I-PMMA)" and solvent-blended PMMA without CNF ("0)" shows a 25 °C reduction, which is likely due, at least in part, to the effects of the residual DMF solvent. This difference is reduced but not eliminated in the second and third heating cycles despite the elevation of the temperature to 200 °C during the heating cycle.

Table 1. T_g Values of the as-Received PMMA (I-PMMA) and PMMA Solvent-Blended with Various Amounts of CNFs with Reported Values for Three Successive Cycles by DSC

CNF content (wt/wt %)	first heating (°C)	second heating (°C)	third heating (°C)
I-PMMA	107	116	118
0	82	102	108
0.5	84	104	109
1	87	103	108
3	89	107	113

Continuous fibers were melt-spun from the as-received PMMA and solvent-blended compounds. Despite the relatively low T_g values, good fibers were unable to be spun from the solvent-blended compounds at melt temperatures below 192 °C, which led to some degradation, in the form of discoloration of CNFs despite nitrogen blanketing. After melt spinning, the fibers were further drawn in the second step at temperatures well below the melt-spinning temperatures. While there is some drawing of the melt during spinning, we use the term draw ratio (DR) to refer to this second draw at colder temperature, with the as-spun fibers having a DR of 1.

FTIR. Figure 1 shows the FTIR (attenuated total reflectance (ATR)) spectra for the fibers made from the as-received and solvent-blended PMMA (I-PMMA and D-PMMA, respectively; DR of 1) as well as the DMF solvent. It is clear from the small peak at 1680 cm^{-1} and the small shoulder at 1093 cm^{-1}

https://doi.org/10.1021/acsapm.1c00933
ACS Appl. Polym. Mater. 2021, 3, 6102−6110

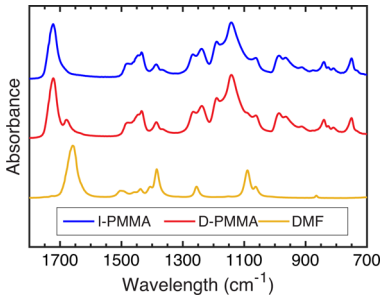

Figure 1. ATR FTIR spectra of as-received PMMA (I-PMMA) fiber, solvent-blended PMMA (D-PMMA) fiber, and DMF solvent. Spectra are offset for visualization.

in the D-PMMA fiber spectra, both because of DMF, that the residual solvent remains despite the careful vacuum drying prior to spinning as well as the high melt-spinning temperatures. Such tightly bound DMF was also noted by Patra et al.[26] in solvent-cast PMMA films.

In vibrational spectroscopy, dichroism has been used to measure the alignment of a variety of materials and often has the ability to assess the alignment of the different components of a composite or blend, for example. In this investigation, we used polarized FTIR spectroscopy to investigate the alignment of CNFs and PMMA within our fibers. Though many of the peaks of CNFs and PMMA overlap, at a sufficiently high CNF content, the peak at 3340 cm^{-1}, one of the hydroxyl stretches of the CNF, was large enough to clearly show dichroism and confirm at least partial alignment of the CNF, even in the as-spun fibers (Figure 2). However, because of overlap with other

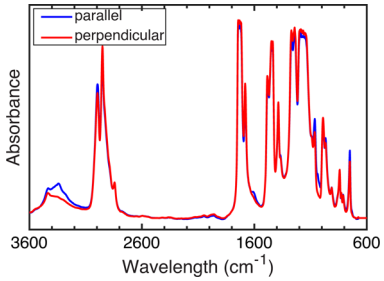

Figure 2. FTIR transmission spectra of a PMMA fiber containing 3% CNF (DR = 1) at different orientations relative to the direction of polarization.

CNF hydroxyl stretches in the same vicinity as well as a small PMMA peak at 3440 cm^{-1}, no attempts were made to quantify the CNF dichroism.

The PMMA skeletal vibration at 749 cm^{-1} was sufficiently isolated to determine a dichroic ratio as a measure of the relative molecular orientation of the PMMA in the fibers. Others have used this band to measure PMMA alignment in oriented films[28] and electrospun fibers[20] made from PMMA-poly(ethylene oxide) blends. All of our as-spun fibers (i.e., DR = 1.0) had dichroic ratios above 1 indicating significant PMMA alignment during melt spinning. Further drawing of PMMA fibers was possible at the lower temperatures used for the secondary drawing, and their dichroic ratios trended well with the DR (Figure 3a). However, for the composite fibers, less drawing was possible, especially at a higher CNF content, and their dichroic ratios were less consistent with those of the PMMA fiber both in terms of the variability and trending with the DR. This is likely due to CNFs forming a percolated network that interfered with the drawing process. The effect of CNF content on the dichroic ratios for the as-spun composite fibers (i.e., DR = 1) is shown in Figure 3b.

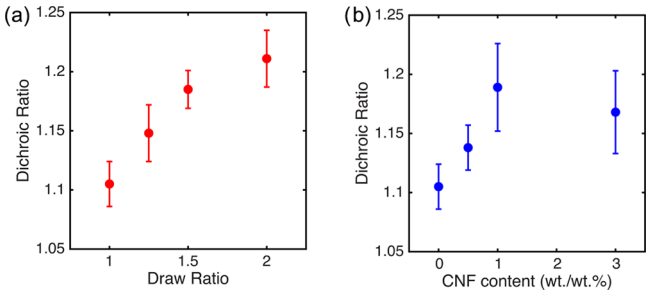

Figure 3. Dichroic ratios of the 749 cm^{-1} PMMA peak with (a) varying DRs at 0% CNF content and (b) varying CNF content at a DR of 1. (Marker = mean and error bar = standard deviation).

Tensile Properties of PMMA-CNF Composite Fibers. Figure 4 shows the variation of Young's modulus and yield

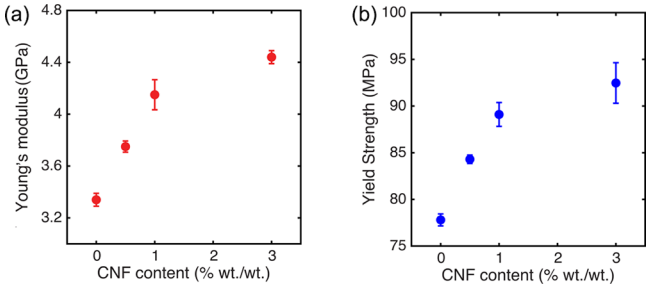

Figure 4. Mechanical properties of PMMA-CNF composite fibers (DR = 1) with different CNF contents: (a) Young's modulus (initial modulus) and (b) yield strength. (Marker = mean and error bar = standard deviation).

strength of the specimens as the composition of the composite fiber is varied. It is evident that the strength and modulus increase with an increase in the CNF content. Modulus and strength increased by 35 and 19%, respectively, when 3% wt CNF was added.

The increase in tensile properties can be attributed to the high modulus and strength of individual nanocellulose fibers, estimated to be 61−107 GPa[29] and 1−3 GPa,[2] respectively. These results suggest that there is good stress transfer between the PMMA matrix and CNFs. The moduli of the composite fibers were compared with predictions from common models for composite moduli. The Voigt[30,31] and Reuss[32] predictions of effective modulus (as summarized by Hill[33]) and a prediction based on Hashin's[34] micromechanical model for statistically isotropic composites, commonly referred to as the Hashin−Shtrikman model, are shown in Figure 5. The Voigt model assumes isostrain, and the Reuss model assumes isostress to calculate the effective composite modulus (stiffness) as a function of composition. The Hashin−Shtrikman model assumes a statistically isotropic composite with arbitrary inclusion-phase geometry for cases in which the matrix contains randomly oriented particles (e.g., short fibers) or spherical particles. Bulk modulus and shear modulus of PMMA-CNF fibers are calculated from Young's modulus and Poisson's ratio (E_1 = 3.34 GPa, E_2 = 80 − 120 GPa, ν_1 = 0.35,

https://doi.org/10.1021/acsapm.1c00933
ACS Appl. Polym. Mater. 2021, 3, 6102−6110

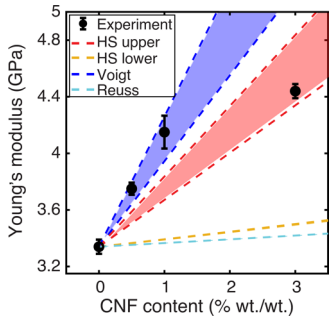

Figure 5. Predictions of effective composite Young's modulus compared with experimental measurements from tensile testing of PMMA-CNF fibers. (H–S: Hashin–Shtrikman and V–R: Voigt–Reuss). Each data point contains 13–19 specimens. (Marker = mean and error bar = standard deviation).

and $\nu_2 = 0.24$[35] where 1 = PMMA, 2 = CNF) and are used in turn to calculate bounds on Young's modulus of the composites in the Hashin–Shtrikman model.

Figure 5 shows the comparison of both the predicted bounds (Hashin–Shtrikman[34] and Voigt–Reuss[31,32]) and the experimental measurements of Young's moduli of the composite fibers. As noted earlier, the increase in mechanical properties suggests effective stress transfer between the matrix and CNF. The Voigt model assumes a geometry in which the reinforcing phase is aligned with the loading direction, leading to constant strain in the matrix and fibers and a significant enhancement of stiffness. For fibers with CNF content up to 1%, the experimental measurements sit close to the Voigt bound (Figure 5), suggesting good dispersion and a high degree of orientation of the CNFs in the fibers. The Voigt upper bound can only be reached if the CNFs are well aligned along the loading direction. The deviation from the Voigt bound at CNF content above 1% wt could be due to the formation of a percolated network of CNFs that reduces CNF alignment and results in decreased homogeneity and dispersion within the fibers. Thus, these modulus measurements combined with the comparisons to the models suggest that at 1% wt and below that the CNFs are well aligned in the loading direction.

Figure 6 shows the variation of Young's modulus with the diameter of the fibers. The modulus exhibited a weak increasing trend with the decrease in the fiber diameter, indicating a modest specimen size effect on the tensile modulus. Given that drawing is part of the fiber preparation process, this trend is not surprising. The smaller diameter

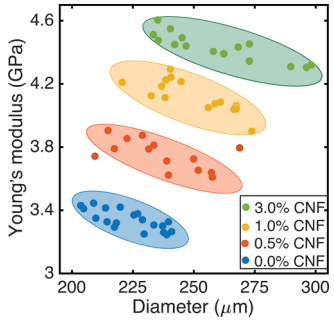

Figure 6. Variation of Young's modulus with the diameter of the composite fibers for different compositions of CNFs highlighting the effect of the specimen size on Young's modulus.

fibers have a higher DR that likely increases the molecular alignment of the PMMA; this, in turn, results in a modest increase in the stiffness (modulus) as the diameter decreases. This type of variation in modulus with the diameter of the fibers was also observed by Pai et al.[36] with their work on poly(trimethyl hexamethylene terephthalamide) fibers. Pai et al. used dichroic ratio measurements using polarized FTIR spectroscopy to measure the molecular orientation and concluded that the increase in alignment and the decrease in diameter account for their observed increased fiber stiffness. While the tensile properties of PMMA-CNF composite fibers vary with the fiber diameter, the variation is approximately ±5% within each data set for fixed CNF content. Figure 6 clearly shows that the CNF content rather than the fiber diameter is the dominant factor in determining Young's modulus.

Fracture Toughness. A typical force–displacement curve from the testing of a notched fiber is shown in Figure 7. Similar

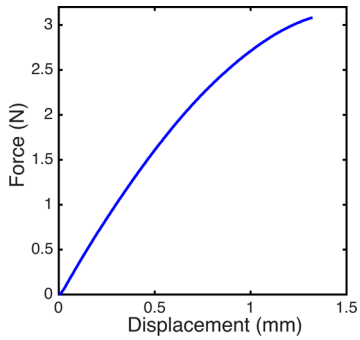

Figure 7. Force–displacement curve of a precracked 1% CNF-PMMA fiber (DR = 1) with a diameter of 216 μm and initial precrack of 55 μm loaded to failure.

behavior was observed in all the tests, with an initial linear behavior followed by a transition to a nonlinear force–displacement response. The fracture surfaces were subsequently imaged by SEM, and select images are shown in Figure 8. A flat precrack surface is clearly observed in Figure 8d. Riverline patterns on the surface where crack propagation occurred are observed in all the specimens. These riverlines emerge from the initial crack front and coalesce to form thicker lines in the direction of crack propagation across the diameter of the fiber, which is typical in the fracture of brittle polymers.[37] Plane strain conditions through most of the middle region of the fiber resulted in a relatively straight crack front in the center of the fiber. The presence of the free surface and the transition to plane stress conditions because of the outer surfaces resulted in a curved crack front at the edges. These observations of riverlines and their coalescence during the initial stage of crack growth and smooth (flat) fracture surfaces as well as low (i.e., room)-temperature testing relative to T_G led to the conclusion that the fiber fracture can be assumed to be brittle,[37] and a linear elastic fracture mechanics-based fracture model was used to determine the fracture toughness.

The mode I fracture toughness K_{IC} is determined from the experimental data from using

$$K_{IC} = \sigma_f Y \sqrt{\pi \cdot a_i} \quad (3)$$

where σ_f is the far-field fracture stress measured in the experiment, a_i is the precrack length, and Y is the geometry

https://doi.org/10.1021/acsapm.1c00933
ACS Appl. Polym. Mater. 2021, 3, 6102–6110

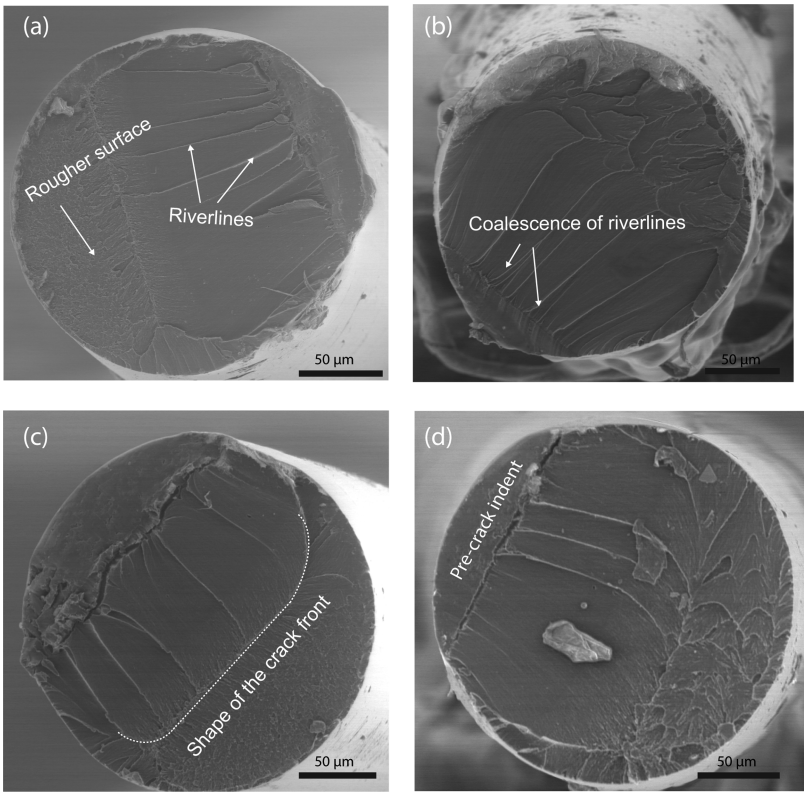

Figure 8. SEM images of the fracture surface of 0.5% ((a) and (b)) and 1% ((c) and (d)) CNF-PMMA composite fibers: (a)−(d) Images of the fracture surfaces showing a straight-faced edge precrack and the crack growth direction indicated by the riverline patterns on the surfaces.

factor. Toribio et al.[38] found that the function plotted in Figure S5 and shown in eq 4[39] provides the closest approximation of the stress intensity factor for the specimen geometry used here

$$Y = 1.4408 - 3.6364\left(\frac{a}{D}\right) + 19.3500\left(\frac{a}{D}\right)^2 - 34.7849\left(\frac{a}{D}\right)^3 + 36.8446\left(\frac{a}{D}\right)^4 \quad (4)$$

where a/D is the ratio of the crack length to fiber diameter. The a/D ratio for each specimen was measured from the SEM images of the fracture surfaces. Fracture stress σ_f (or the far-field stress at fracture) was determined from the peak load in the force−displacement curves and the cross-sectional area. The initial crack length was used as the critical crack length at fracture as it was observed in videos of the tests that catastrophic failure occurs at this crack length.

Figure 9 shows the fracture toughness K_{IC} as a function of CNF content (DR = 1). The measured fracture toughness of pure PMMA fibers (no CNF) agrees with previous work on the fracture toughness of PMMA sheets (0.85 − 0.90 MPa$\sqrt{m}$ for PMMA with a M_W of 120,000).[40] Significantly, the fracture toughness increases by nearly a factor of two relative to the neat PMMA because of the addition of 1 wt % CNF. The fracture toughness of the 3 wt % CNF fibers is not significantly different from that the 1 wt % CNF specimens. The modulus and strength data presented above showed a similar trend—CNF weight fractions up to 1% resulted in significant mechanical enhancement while the higher wt % resulted in minimal further improvement. As noted earlier, this may be due to the CNFs forming a percolated network at 3 wt %, thus resulting in the CNFs having less orientation in the fibers.

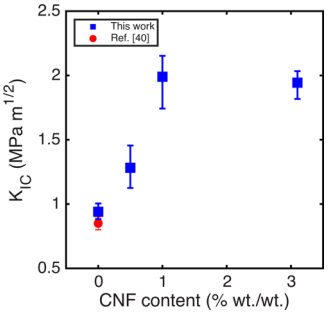

Figure 9. Measured fracture toughness, K_{IC}, of PMMA-CNF fibers. Fracture data on PMMA sheets with a comparable molecular weight (M_W) from Kim et al.[40] are shown for comparison. Each data point represents 4−5 specimens. (Marker = median and error bar = standard deviation).

The dichroic ratio data in Figure 3b suggest that the PMMA alignment increases with increasing CNF content up to 1 wt %. Thus, to understand if the enhancement in toughness with CNFs (Figure 9) was simply due to alignment of the PMMA chains, additional tests were conducted to measure K_{IC} of neat PMMA fibers as a function of DR. As shown in Figure 10, K_{IC} increases with the DR, but the peak fracture toughness reached is about 1.4 MPa$\sqrt{m}$ which is less than the fracture toughness of 1.9 MPa$\sqrt{m}$ measured for PMMA fibers with 1% CNF. The dichroic ratios for the more highly drawn neat PMMA fibers are comparable to the dichroic ratios of the 1 wt % CNF fibers (Figure 3); this suggests that the toughness enhancement resulting from CNF reinforcement cannot be attributed to molecular alignment alone. Previous studies on the effect of molecular alignment on fracture toughness found little to

https://doi.org/10.1021/acsapm.1c00933
ACS Appl. Polym. Mater. 2021, 3, 6102−6110

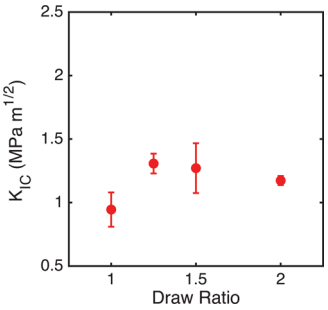

Figure 10. K_{IC} fracture toughness of neat PMMA fibers as a function of DR.

modest effect. Zhao et al.[41] found no clear effect of in-plane PMMA orientation on the fracture toughness of bi-axially oriented PMMA, while Gotham and Scrutton[42] showed that fracture toughness can differ by 35% between crack propagation along the direction of alignment and perpendicular to the alignment.

Thus, the increase in fracture toughness of the PMMA-CNF composites up to 1 wt % is likely due to a combination of molecular alignment and toughening to the presence of the fibers. In particular, crack bridging by CNFs and dissipation because of CNF pullout, which are common in high aspect ratio fiber-reinforced composite materials,[10,14] likely contribute to the observed toughening. The formation of a CNF network or agglomerates may be the reason for the lack of increase in fracture toughness above 1% wt; this was also observed in other studies on PMMA-CNT[43] and PMMA-CNF[5,14] composites. Though different from fracture toughness, Dong et al.[14] found that the tensile toughness and failure strain increased when up to 3 wt % CNF was added to PMMA films, but values decreased upon further addition of CNF. Nanofibrils were observed extending from the fracture surfaces, suggesting the fiber pullout mechanism. Other research studies on similar composites by Shih et al.,[44] Kiziltas et al.,[13] Banerjee et al.,[15] and Santamarti et al.[45] only looked at the effects of CNF content on tensile modulus, strength, and elongation at break but not fracture toughness.

CONCLUSIONS

Composite fibers made of PMMA and CNFs were prepared by a melt-spinning technique. However, the combination of high processing temperatures of PMMA and the low thermal stability of CNFs is problematic when subjecting their combinations to melt processing. Additionally, our processing results show that the network structure formed by percolation of the CNF can limit the ability of the fiber to be drawn. While melt processing is a common, efficient method for thermoplastic composite fabrication and was possible for our PMMA-CNF composites, other preparation methods should be explored that better accommodate material requirements and limitations. Measurement of elastic modulus and yield strength using custom-designed fixtures found an increase in mechanical properties with increasing CNF content up to 3 wt %, which can be largely explained by polymer orientation and effective two-phase theoretical composite theories. Fracture toughness measurements were performed by fabricating precracks via indentation of the fiber producing straight-face edge cracks. A doubling of the fracture toughness was observed with addition of 1 wt % CNF content, and this increase can be attributed to toughening mechanisms such as fiber pullout and crack bridging. Importantly, adding CNFs as a reinforcing agent leads to an increase in strength and modulus, while simultaneously increasing the fracture toughness.

ASSOCIATED CONTENT

Supporting Information

The Supporting Information is available free of charge at https://pubs.acs.org/doi/10.1021/acsapm.1c00933.

Figures showing custom fixtures to mount fibers, representative tensile stress−strain curves, schematic of the precrack cross section of the fiber, dichroic ratio measurements, and Valiente's nondimensional SIF and mathematical framework behind the composite bound models (PDF)

AUTHOR INFORMATION

Corresponding Author

Kevin T. Turner − *Department of Mechanical Engineering and Applied Mechanics, University of Pennsylvania, Philadelphia, Pennsylvania 19104, United States;* orcid.org/0000-0003-4963-4568; Email: kturner@seas.upenn.edu

Authors

Gnana Saurya Vankayalapati − *Department of Mechanical Engineering and Applied Mechanics, University of Pennsylvania, Philadelphia, Pennsylvania 19104, United States*

Ethan Kaplan − *Department of Mechanical Engineering and Applied Mechanics, University of Pennsylvania, Philadelphia, Pennsylvania 19104, United States*

Lisa M. Lallo − *Department of Mechanical Engineering and Applied Mechanics, University of Pennsylvania, Philadelphia, Pennsylvania 19104, United States; Currently at Exponent, Inc., Philadelphia, Pennsylvania 19104, United States*

Nikhil Victor − *USDA Forest Products Laboratory, Madison, Wisconsin 53726, United States;* Present Address: Pyran Inc., Madison, Wisconsin 53719, United States

Craig M. Clemons − *USDA Forest Products Laboratory, Madison, Wisconsin 53726, United States*

John M. Considine − *USDA Forest Products Laboratory, Madison, Wisconsin 53726, United States*

Complete contact information is available at: https://pubs.acs.org/10.1021/acsapm.1c00933

Notes

The authors declare no competing financial interest.

ACKNOWLEDGMENTS

This work is supported by the USDA National Institute of Food and Agriculture, AFRI project 2017-67021-26601. Additional support was provided by U.S. Endowment for Forestry & Communities, Inc. as part of the P3Nano program. This work was performed in part at the University of Pennsylvania's Singh Center for Nanotechnology, an NNCI member supported by NSF Grant ECCS-1542153. The authors appreciate Yash Daswani (University of Pennsylvania) for help with preliminary tensile testing and Gokulanand Iyer (University of Pennsylvania) for help with assembling the microindentation setup used for precracking. The authors would also like to thank Prof. John L. Bassani and Sumukh

Shankar Pande (University of Pennsylvania) for helpful discussions about polymer and fiber fracture.

REFERENCES

(1) Fukuzumi, H.; Saito, T.; Iwata, T.; Kumamoto, Y.; Isogai, A. Transparent and High Gas Barrier Films of Cellulose Nanofibers Prepared by TEMPO-Mediated Oxidation. *Biomacromolecules* **2009**, *10*, 162−165.
(2) Isogai, A. Wood Nanocelluloses: Fundamentals and Applications as New Bio-Based Nanomaterials. *J. Wood Sci.* **2013**, *59*, 449−459.
(3) Ozgur Seydibeyoglu, M.; Oksman, K. Novel Nanocomposites Based on Polyurethane and Micro Fibrillated Cellulose. *Compos. Sci. Technol.* **2008**, *68*, 908−914.
(4) Leng, W.; Pan, B. Thermal Insulating and Mechanical Properties of Cellulose Nanofibrils Modified Polyurethane Foam Composite as Structural Insulated Material. *Forests* **2019**, *10*, 200.
(5) Zhang, C.; Zhai, T.; Sabo, R.; Clemons, C.; Dan, Y.; Turng, L.-S. Reinforcing Natural Rubber with Cellulose Nanofibrils Extracted from Bleached Eucalyptus Kraft Pulp. *J. Biobased Mater. Bioenergy* **2014**, *8*, 317−324.
(6) Venugopal, B.; Gopalakrishnan, J. Reinforcement of Natural Rubber Using Cellulose Nanofibres Isolated from Coconut Spathe. *Mater. Today: Proc.* **2018**, *5*, 16724−16731.
(7) Ritchie, R. O. The Conflicts between Strength and Toughness. *Nat. Mater.* **2011**, *10*, 817−822.
(8) Bhattacharya, M. Polymer Nanocomposites—A Comparison between Carbon Nanotubes, Graphene, and Clay as Nanofillers. *Materials* **2016**, *9*, 262.
(9) Vallittu, P. K. High-Aspect Ratio Fillers: Fiber-Reinforced Composites and Their Anisotropic Properties. *Dent. Mater.* **2015**, *31*, 1−7.
(10) Gojny, F. H.; Wichmann, M. H. G.; Köpke, U.; Fiedler, B.; Schulte, K. Carbon Nanotube-Reinforced Epoxy-Composites: Enhanced Stiffness and Fracture Toughness at Low Nanotube Content. *Compos. Sci. Technol.* **2004**, *64*, 2363−2371.
(11) Hsieh, T. H.; Kinloch, A. J.; Taylor, A. C.; Kinloch, I. A. The Effect of Carbon Nanotubes on the Fracture Toughness and Fatigue Performance of a Thermosetting Epoxy Polymer. *J. Mater. Sci.* **2011**, *46*, 7525−7535.
(12) Sui, X.; Wagner, H. D. Tough Nanocomposites: The Role of Carbon Nanotube Type. *Nano Lett.* **2009**, *9*, 1423−1426.
(13) Kiziltas, A.; Nazari, B.; Kiziltas, E. E.; Gardner, D. J. S.; Han, Y.; Rushing, T. S. Cellulose NANOFIBER-Polyethylene Nanocomposites Modified by Polyvinyl Alcohol. *J. Appl. Polym. Sci.* **2016**, *133*, No. 42933.
(14) Dong, H.; Sliozberg, Y. R.; Snyder, J. F.; Steele, J.; Chantawansri, T. L.; Orlicki, J. A.; Walck, S. D.; Reiner, R. S.; Rudie, A. W. Highly Transparent and Toughened Poly(Methyl Methacrylate) Nanocomposite Films Containing Networks of Cellulose Nanofibrils. *ACS Appl. Mater. Interfaces* **2015**, *7*, 25464−25472.
(15) Banerjee, M.; Sain, S.; Mukhopadhyay, A.; Sengupta, S.; Kar, T.; Ray, D. *Surface Treatment of Cellulose Fibers with Methylmethacrylate for Enhanced Properties of in Situ Polymerized PMMA/Cellulose Composites*. J. Appl. Polym. Sci. 2014, *131* (2), DOI: 10.1002/app.39808.
(16) Oliver-Ortega, H.; Geng, S.; Espinach, F. X.; Oksman, K.; Vilaseca, F. Bacterial Cellulose Network from Kombucha Fermentation Impregnated with Emulsion-Polymerized Poly(Methyl Methacrylate) to Form Nanocomposite. *Polymer* **2021**, *13*, 664.
(17) Reiner, R. S. *Process Scale-Up of Cellulose Nanocrystal Production to 25 Kg per Batch at the Forest Products Laboratory*. 6.
(18) Mariani, L. M.; Johnson, W. R., III; Considine, J. M.; Turner, K. T. Printing and Mechanical Characterization of Cellulose Nanofibril Materials. *Cellulose* **2019**, *26*, 2639−2651.
(19) D20 Committee. *Test Method for Transition Temperatures and Enthalpies of Fusion and Crystallization of Polymers by Differential Scanning Calorimetry*; ASTM International.
(20) Andersson, R. L.; Ström, V.; Gedde, U. W.; Mallon, P. E.; Hedenqvist, M. S.; Olsson, R. T. Micromechanics of Ultra-Toughened Electrospun PMMA/PEO Fibres as Revealed by *in-Situ* Tensile Testing in an Electron Microscope. *Sci. Rep.* **2015**, *4*, 6335.
(21) C28 Committee. *Test Method for Tensile Strength and Youngs Modulus of Fibers*; ASTM International.
(22) Adusumalli, R.-B.; Muller, U.; Weber, H.; Roeder, T.; Sixta, H.; Gindl, W. Tensile Testing of Single Regenerated Cellulose Fibres. *Macromol. Symp.* **2006**, *244*, 83−88.
(23) Kant, M.; Penumadu, D. Fracture Behavior of Individual Carbon Fibers in Tension Using Nano-Fabricated Notches. *Compos. Sci. Technol.* **2013**, *89*, 83−88.
(24) Suhling, J. C.; Johnson, M. W.; Rowlands, R. E.; Gunderson, D. E. *Nonlinear Elastic Constitutive Relations for Cellulosic Materials*. 13.
(25) Baez, C.; Considine, J.; Rowlands, R. Influence of Drying Restraint on Physical and Mechanical Properties of Nanofibrillated Cellulose Films. *Cellulose* **2014**, *21*, 347−356.
(26) Patra, N.; Barone, A. C.; Salerno, M. Solvent effects on the thermal and mechanical properties of poly (methyl methacrylate) casted from concentrated solutions. *Adv. Polym. Technol.* **2011**, *30*, 12−20 Wiley Online Library(accessed 2019 -11 -07)..
(27) Patra, N.; Salerno, M.; Diaspro, A.; Athanassiou, A. Effect of Solvents on the Dynamic Viscoelastic Behavior of Poly(Methyl Methacrylate) Film Prepared by Solvent Casting. *J. Mater. Sci.* **2011**, *46*, 5044−5049.
(28) Zhao, Y.; Jasse, B.; Monnerie, L. Orientation and Relaxation in Uniaxially Stretched Poly(Methyl Methacrylate)-Poly (Ethylene Oxide) Blends. *Polymer* **1989**, *30*, 1643−1650.
(29) Cheng, Q.; Wang, S.; Harper, D. P. Effects of Process and Source on Elastic Modulus of Single Cellulose Fibrils Evaluated by Atomic Force Microscopy. *Compos. Part A: Appl. Sci. Manuf.* **2009**, *40*, 583−588.
(30) Liu, B.; Feng, X.; Zhang, S.-M. The Effective Young's Modulus of Composites beyond the Voigt Estimation Due to the Poisson Effect. *Compos. Sci. Technol.* **2009**, *69*, 2198−2204.
(31) Voigt, W. *Lehrbuch der Kristallphysik*; Vieweg+Teubner Verlag, 1966.
(32) Reuss, A. Berechnung der Fließgrenze von Mischkristallen auf Grund der Plastizitatsbedingung fur Einkristalle. *Z. Angew. Math. Mech.* **1929**, *9*, 49−58.
(33) Hill, R. The Elastic Behaviour of a Crystalline Aggregate. *Proc. Phys. Soc. A* **1952**, *65*, 349.
(34) Hashin, Z. Analysis of Composite Materials—A Survey. *J. Appl. Mech.* **1983**, *50*, 481−505.
(35) Josefsson, G.; Berthold, F.; Gamstedt, E. K. Stiffness Contribution of Cellulose Nanofibrils to Composite Materials. *Int. J. Solids Struct.* **2014**, *51*, 945−953.
(36) Pai, C.-L.; Boyce, M. C.; Rutledge, G. C. Mechanical Properties of Individual Electrospun PA 6(3)T Fibers and Their Variation with Fiber Diameter. *Polymer* **2011**, *52*, 2295−2301.
(37) Hayes, M.; Edwards, D.; Shah, A. *Fractography in Failure Analysis of Polymers*; Elsevier Science & Technology Books: Oxford, United States, 2015.
(38) Toribio, J.; Alvarez, N.; González, B.; Matos, J. C. A Critical Review of Stress Intensity Factor Solutions for Surface Cracks in Round Bars Subjected to Tension Loading. *Eng. Fail. Anal.* **2009**, *16*, 794−809.
(39) Valiente Cancho, A. *Criterios de fractura para alambres*. phd, E.T.S.I. Caminos, Canales y Puertos (UPM), 1980.
(40) Kim, S. L.; Skibo, M.; Manson, J. A.; Hertzberg, R. W. Fatigue crack propagation in poly (methyl methacrylate): Effect of molecular weight and internal plasticization. *Polym. Eng. Sci.* **1977**, *17*, 194−203 Wiley Online Library(accessed 2019-11-25)..
(41) Zhao, J. Y.; Blackman, B.; Patel, Y.; Yan, Y. The Fracture Resistance of Bi-Axially Orientated PMMA. *IOP Conf. Ser.: Mater. Sci. Eng.* **2020**, *770*, 012025.
(42) Gotham, K. V.; Scrutton, I. N. Effect of Molecular Orientation on the Fracture Toughness of Thermoplastics. *Polymer* **1978**, *19*, 341−347.

https://doi.org/10.1021/acsapm.1c00933
ACS Appl. Polym. Mater. 2021, 3, 6102−6110

(43) Blond, D.; Barron, V.; Ruether, M.; Ryan, K. P.; Nicolosi, V.; Blau, W. J.; Coleman, J. N. Enhancement of Modulus, Strength, and Toughness in Poly(methyl methacrylate)-Based Composites by the Incorporation of Poly(methyl methacrylate)-Functionalized Nanotubes. *Adv. Funct. Mater.* **2006**, *16*, 1608−1614 Wiley Online Library(accessed 2019-11-25)..

(44) Shih, Y. F.; Chou, M. Y.; Lian, H. Y.; Hsu, L. R.; Chen-Wei, S. M. Highly Transparent and Impact-Resistant PMMA Nanocomposites Reinforced by Cellulose Nanofibers of Pineapple Leaves Modified by Eco-Friendly Methods. *Express Polym. Lett.* **2018**, *12*, 844−854.

(45) Santmarti, A.; Teh, J. W.; Lee, K.-Y. Transparent Poly(Methyl Methacrylate) Composites Based on Bacterial Cellulose Nanofiber Networks with Improved Fracture Resistance and Impact Strength. *ACS Omega* **2019**, *4*, 9896−9903.

https://doi.org/10.1021/acsapm.1c00933
ACS Appl. Polym. Mater. 2021, 3, 6102−6110